IEEE TRANSACTIONS ON

ELECTROMAGNETIC COMPATIBILITY

A PUBLICATION OF THE IEEE ELECTROMAGNETIC COMPATIBILITY SOCIETY

EMC SOCIETY

FEBRUARY 2016 VOLUME 58 NUMBER 1 IEMCAE (ISSN 0018-9375)

(Contents Continued on Page 1)

IEEE

IEEE TRANSACTIONS ON ELECTROMAGNETIC COMPATIBILITY (ISSN 0018-9375) is published bimonthly by the Institute of Electrical and Electronics Engineers, Inc. Responsibility for the contents rests upon the authors and not upon the IEEE, the Society/Council, or its members. **IEEE Corporate Office**: 3 Park Avenue, 17th Floor, New York, NY 10016-5997. **IEEE Operations Center:** 445 Hoes Lane, Piscataway, NJ 08854-4141. **NJ Telephone**: +1 732 981 0060. **Price/Publication Information:** Individual copies: IEEE Members $50.00 (first copy only), nonmembers $80.00 per copy. (Note: Postage and handling charge not included.) Member and nonmember subscription prices available upon request.

Periodicals Postage Paid at New York, NY and at additional mailing offices. **Postmaster:** Send address changes to IEEE TRANSACTIONS ON ELECTROMAGNETIC COMPATIBILITY, IEEE, 445 Hoes Lane, Piscataway, NJ 08854-4141. GST Registration No. 125634188. CPC Sales Agreement #40013087. Return undeliverable Canada addresses to: Pitney Bowes IMEX, P.O. Box 4332, Stanton Rd., Toronto, ON M5W 3J4, Canada. IEEE prohibits discrimination, harassment and bullying. For more information visit http://www.ieee.org/nondiscrimination. Printed in U.S.A.

Digital Object Identifier 10.1109/TEMC.2016.2526979

On the Image Model of a Buried Horizontal Wire

Vesna Arnautovski-Toseva, *Member, IEEE*, and Leonid Grcev, *Fellow, IEEE*

***Abstract*—It is common practice in the engineering analysis process to use an approximate image method for the computation of the current in buried horizontal conductors (in the literature, this is often referred to as the "modified image" or "reflection coefficient" method). According to this approach, the earth/air interface is replaced by a positive mirror image of the charge and current in the conductor, and its field is multiplied by a suitable reflection coefficient. Different opinions on the validity of this approximation have been expressed in published debates, but more systematic analysis of the error introduced by this approach is not available in the literature. To establish the amount of error, we compare the computation results of the image model with the rigorous Sommerfeld integral method for a wide range of parameters. Contrary to widespread opinion, our results suggest that the modified image (or reflection coefficient) method in EFIE-based solutions (e.g., the Pocklington equation) leads to a large error (larger than 20%) in the low-frequency range for the computation of the current distribution in conductors longer than 10 m. In such a case, MPIE-based methods are preferred for use to achieve a smaller error (approximately 5%). Guidelines for the application of image models related to the conductor, earth and excitation parameters, upper frequency limit, and modeling method are presented.**

***Index Terms*—Antennas, electromagnetic analysis, frequency response, Green functions, grounding, integral equations, modeling, nonhomogeneous media, reflection coefficient.**

I. Introduction

THE traditionally accepted practice in engineering analysis is to use an approximate image formulation for the computation of the current in buried horizontal wires of finite length (such formulation is often referred to in the literature as the "modified image" or "reflection coefficient" method). In this method, the air half-space is replaced with a positive mirror image of the charge and longitudinal current distribution along the wire above the earth/air interface. The field of the image source is then multiplied by a suitable reflection coefficient. Such an approximate approach was initially applied at low frequencies but is presently applied over a wide frequency range in many areas of electrical engineering, e.g., electric power systems, EMC, lightning protection, subsurface communications, geophysical prospecting, etc., [1]–[9].

The idea for this approximation stems from the exact image solutions for dc sources in conducting half-space [10]. The current distribution in buried conductors is determined by the electric field component tangential to the conductors' surface due to the charge and current sources in the conductor. The dc electric field component is exactly determined solely by charge and image theory. With the rise of the frequency, additional electric field component due to current in the conductor becomes important [11]. However, for this component, there is a difference in the image model between vertical and horizontal conductors: the dc vertical current has an image [12], whereas the horizontal current does not [13]. Therefore, a natural extension of the image theory for horizontal conductors in a quasi-static range would be to use an image for the charge, but not for the current. Nevertheless, in the most cases, the solutions are based on the electric field integral equation (EFIE) (e.g., Pocklington equation), which uses images of both charge and current, e.g., [5]–[9]. The use of an image only for the charge is possible in solutions based on the mixed potential integral equation (MPIE) [14].

Contrary to the above approach, Wait, in the debate with Sali [18]–[22], has claimed that a buried current-carrying conductor does not have proper image and that the simple mirror image model should not be used in analysis of buried wires. Nevertheless, confidence in the image models was built on the fact that the computation results (especially in grounding analysis) have been found to be in a reasonable agreement with some experimental results, e.g., [8], [15]–[17]. However, more systematic analysis of the error introduced by this approximate formulation is not available in the literature.

The aim of this paper is to explore the validity of the image models by analyzing the error of the computed current distribution in buried horizontal wires of finite length for various types of excitation. To establish such an error, we compare two image models (first, with images of both current and charge, and, second, with a single image of charge) using as a standard the rigorous Sommerfeld integral method ([14], [23]–[25], [31], [32]). We compare the models over a wide frequency range (from dc to 100 MHz), different earth conductivities (from 0.1 to 0.001 S/m), different wire lengths (from 1 to 100 m), and different burial depths (from 0.3 to 1 m). For all cases, we apply alternatively two types of excitation: first, with a serial voltage generator at the wire's middle point, and second, with illumination by an incident plane wave. In this paper, we analyze only the simplest implementation of the image method, where the air half-space is replaced by a positive mirror image. Here, we do not consider more complex image models, e.g., exact image [26] or discrete complex image models [27]. These approaches and cases for multilayered earth, the frequency dependence of the earth electrical parameters [28], the complete field, and more complicated electrode arrangements (that employ both horizontal and vertical conductors) will be considered in later work.

Manuscript received April 10, 2015; revised October 10, 2015 and August 10, 2015; accepted November 10, 2015. Date of publication December 25, 2015; date of current version February 16, 2016. This work was supported in part by the Macedonian Academy of Sciences and Arts.

V. Arnautovski-Toseva is with the Faculty of Electrical Engineering and Information Technologies, Saints Cyril and Methodius University, Skopje 1000, Macedonia (e-mail: atvesna@feit.ukim.edu.mk).

L. Grcev is with the Faculty of Electrical Engineering and Information Technologies, Saints Cyril and Methodius University, Skopje 1000, Macedonia, and also with the Macedonian Academy of Sciences and Arts, Skopje 1000, Macedonia (e-mail: Leonid.Grcev@ieee.org).

Digital Object Identifier 10.1109/TEMC.2015.2506608

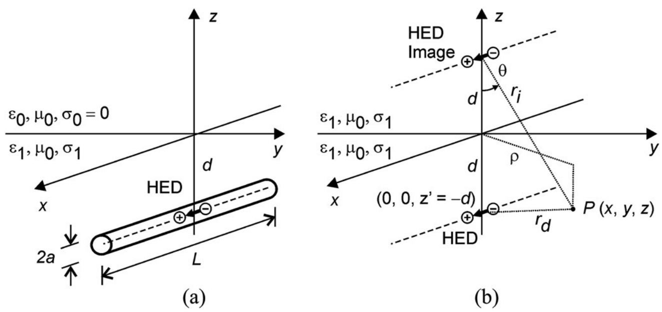

Fig. 1. Illustration of the coordinate system and the position of the buried horizontal wire. (a) Original problem. (b) Image model: HED and its image in unbounded conducting space with the characteristics of earth (ε_1, μ_0, σ_1).

II. MPIE and the Method of Moments

The details of the rigorous Sommerfeld integral model for currents in thin-wire conductors in conductive media based on MPIE may be found elsewhere, e.g., [33]–[36]. Here, we briefly summarize the main steps in the development.

A. Mixed Potential Integral Equation

The physical situation and the coordinate system are illustrated in Fig. 1. The interface between the air and the earth is the plane $z = 0$, with the positive z-direction directed upward into the air. The earth is assumed to be a homogeneous medium characterized by corresponding values of permittivity ε_1, conductivity σ_1, and permeability of vacuum μ_0. We consider a horizontal wire of length L along the x-axis, with radius a buried at depth d. The wire excitation is provided by a harmonic voltage source connected serially at the central point of the wire or alternatively by illumination by a harmonic plane wave of normal incidence. (The time variation $e^{j\omega t}$ is assumed and suppressed.)

Assuming the thin-wire approximation, the equivalent current and charge sources in the wire (see Fig. 1) are approximated by filaments at the wire axis. The boundary condition is satisfied approximately by requiring that only the x-component of the tangential known impressed electric field E_x^i vanishes at the wire surface [29]. We use the well-known MPIE

$$E_x^i = j\omega\mu_0 \int_L G_A I(x')dx' - \frac{1}{j\omega\hat{\varepsilon}_1}\frac{\partial}{\partial x}\int_L G_V \frac{\partial I(x')}{\partial x}dx'$$
$$\hat{\varepsilon}_1 = \varepsilon_1 + \frac{\sigma_1}{j\omega}. \tag{1}$$

Here, $I(x')$ is an unknown filament longitudinal current and G_A and G_V are Green functions of the x-component of the magnetic vector potential and the electric scalar potential, respectively. The integrals superimpose effects of horizontal electric dipoles (HED) (illustrated in Fig. 1) along the conductor axis. G_A and G_V are the result of point current and point charge sources associated with x-oriented HED, respectively (they will be evaluated in next sections of this paper). MPIE (1) allows for application of images separately for the equivalent longitudinal currents and charges because the charge appears explicitly in the evaluation of G_V.

B. Method of Moments

The first step of the application of the method of moments [29] is to assume that the wire is divided into a number of fictitious subsections over which the unknown current is approximated by a sequence of N basis functions [30]. Our choice of the method for numerical solution of the integral (1) is the Galerkin solution with triangular basis and test functions T_n [30]. As a result, the integral equation is reduced to a matrix equation

$$[Z]\cdot[I] = [V]. \tag{2}$$

Here, the elements of the column matrix $[I]$ are the amplitudes of the triangular basis functions, and the elements of $[V]$ are related to the excitation of the wire. Definition of the elements of $[V]$ for excitation with serial voltage generator and with illumination by plane wave can be found elsewhere [29]. The elements of the generalized impedance matrix $[Z]$ describe the electromagnetic interactions between subsections m and n (with lengths ℓ_m and ℓ_n, respectively)

$$z_{mn} = j\omega\mu_0 \int_{\ell_n} T_n dx \int_{\ell_m} G_A T_m dx' + \frac{1}{j\omega\hat{\varepsilon}_1}\int_{\ell_n}\frac{dT_n}{dx}dx \int_{\ell_m} G_V \frac{dT_m}{dx'}dx'. \tag{3}$$

The problem is practically reduced to evaluation of Green functions G_A and G_V.

III. Rigorous Sommerfeld Integral Method

A. Green Functions in the Spectral Domain

We start the analysis of the Green functions in the spectral domain. The interested reader may find details of the development of this solution elsewhere, for example, in [33]–[36]. We consider the x-component field due to a Hertzian HED of unit strength $(Idx = 1\,\mathrm{A}\cdot\mathrm{m})$ that is located at $(0,\,0,\,z')$ and pointed in the x-direction. The field is observed in point P at $(x,\,y,\,z<0)$. The coordinate system is illustrated in Fig. 1(b).

The spectral expressions for the magnetic vector potential Green function $\tilde{G}_A$ and the electric scalar potential Green function $\tilde{G}_V$ in the case when both the source HED and the observation point are in the earth are

$$\tilde{G}_A = \frac{1}{2}\left[\frac{e^{-jk_{z1}|z-z'|}}{jk_{z1}} + R_{\mathrm{TE}}^{10}\frac{e^{-jk_{z1}|z+z'|}}{jk_{z1}}\right] \tag{4}$$

$$\tilde{G}_V = \frac{1}{2}\left[\frac{e^{-jk_{z1}|z-z'|}}{jk_{z1}} + \frac{k_{z1}^2 R_{\mathrm{TM}}^{10} + k_1^2 R_{\mathrm{TE}}^{10}}{k_\rho^2}\frac{e^{-jk_{z1}|z+z'|}}{jk_{z1}}\right] \tag{5}$$

$$R_{\mathrm{TE}}^{10} = \frac{jk_{z1} - jk_{z0}}{jk_{z1} + jk_{z0}}, R_{\mathrm{TM}}^{10} = \frac{\varepsilon_0 jk_{z1} - \hat{\varepsilon}_1 jk_{z0}}{\varepsilon_0 jk_{z1} + \hat{\varepsilon}_1 jk_{z0}}$$
$$k_{z0} = \sqrt{k_0^2 - k_\rho^2}, k_{z1} = \sqrt{k_1^2 - k_\rho^2}, k_\rho = \sqrt{k_x^2 + k_y^2}$$
$$k_0 = \omega\sqrt{\mu_0\varepsilon_0}, k_1 = \omega\sqrt{\mu_0\hat{\varepsilon}_1} \tag{6}$$

where R^{10}_{TE} and R^{10}_{TM} are the Fresnel TE and TM reflection coefficients [37]. Here, $\rho = \sqrt{x^2 + y^2}$ is the radial distance between the HED and the field evaluation point.

B. Green Functions in the Spatial Domain

The spatial expressions for G_A and G_V can be determined by means of the 2-D inverse Fourier transform of their spectral pairs (4), (5) in the form of the well-known Sommerfeld integral [35]:

$$G_{A,V} = \frac{1}{2\pi}\int_0^\infty \tilde{G}_{A,V} J_0(k_\rho \rho) k_\rho dk_\rho \tag{7}$$

where $J_0(\cdot)$ is the Bessel function of the first kind and zero order. The first terms in (4) and (5) have closed-form solutions (obtained by using the Sommerfeld identity) [24], while the other terms are determined by direct numerical integration in a similar manner to the approach used by Burke [25]:

$$G_A = g_d + \frac{1}{4\pi}\int_0^\infty R^{10}_{\mathrm{TE}} \frac{e^{-jk_{z1}|z+z'|}}{jk_{z1}} J_0(k_\rho \rho) k_\rho dk_\rho \tag{8}$$

$$\begin{aligned} G_V = {}& g_d + \frac{1}{4\pi}\int_0^\infty \frac{k_{z1}^2 R^{10}_{\mathrm{TM}} + k_1^2 R^{10}_{\mathrm{TE}}}{k_\rho^2} \\ & \times \frac{e^{-jk_{z1}|z+z'|}}{jk_{z1}} J_0(k_\rho \rho) k_\rho dk_\rho \end{aligned} \tag{9}$$

$$g_d = \frac{1}{4\pi}\frac{e^{-jk_1 r_d}}{r_d}. \tag{10}$$

Here, g_d is the direct field term that represents the spherical wave arising in the case when the HED is in an infinite homogeneous medium with the characteristics of the earth.

IV. Image Approximation

Image approximation of the Green functions follows from an approximation at low frequencies. When $\omega \to 0$ the following approximation $jk_{z1} \approx jk_{z0}$ is valid because $k_\rho^2 >> k_0^2$ and $k_\rho^2 >> k_1^2$. By substitution into (6), we obtain the following low-frequency approximation of the Fresnel reflection coefficients

$$R^{10}_{\mathrm{TM}} = -K_{10}, R^{10}_{\mathrm{TE}} = 0 \tag{11}$$

and

$$K_{10} = \frac{\hat{\varepsilon}_1 - \varepsilon_0}{\hat{\varepsilon}_1 + \varepsilon_0}. \tag{12}$$

Here, K_{10} is the quasi-static Fresnel reflection coefficient for a normal plane wave. This is a key simplification because K_{10} is a constant, which enables the derivation of closed-form solution of the integral in (9). Substitution of (11), (12) into (8), (9) gives image approximation of the Green functions

$$G_A = g_d \tag{13}$$

$$\begin{aligned} G_V &= g_d + K_{10}\frac{1}{4\pi}\int_0^\infty \frac{e^{-jk_{z1}|z+z'|}}{jk_{z1}} J_0(k_\rho \rho) k_\rho dk_\rho \\ &= g_d + K_{10} g_i \end{aligned} \tag{14}$$

$$g_i = \frac{1}{4\pi}\frac{e^{-jk_1 r_i}}{r_i}. \tag{15}$$

Here, g_i is the image field term that represents a spherical wave that arises in the case when the HED is its image position [see Fig. 1(b)]. Therefore, only charge sources associated with HED have modified images in (14), while there is no image due to current for the *x*-component of G_A (13). The same conclusion is also obtained in [13], where the solution is derived for a frequency limit at dc.

V. Analyzed Image Models

In the next section we compare two different image models with the rigorous Sommerfeld integral model.

A. Charge Image Model

The first model (referred in next sections as "CHARGE IMAGE") (13)–(15) is derived in the previous Sections as the low-frequency approximation of the rigorous Sommerfeld integral solution:

$$G_A = g_d, G_V = g_d + K_{10} g_i. \tag{16}$$

This model was utilized in the MPIE based solution [14].

B. Modified Image Model

The second image model (referred in next sections as "MODIFIED IMAGE"), which is introduced in [8], has images of both current and charge multiplied by quasi-static Fresnel reflection coefficient for a normal plane-wave K_{10} (12):

$$G_A = g_d + K_{10} g_i, \; G_V = g_d + K_{10} g_i. \tag{17}$$

Another possibility is to use different forms of the quasi-static Fresnel reflection coefficient, that is, for an oblique plane-wave Γ_{10} instead of K_{10} (12) in (17), e.g., [5], [9]:

$$\Gamma_{10} = \frac{\cos\theta - \eta\sqrt{1-\eta^2\sin^2\theta}}{\cos\theta + \eta\sqrt{1-\eta^2\sin^2\theta}}, \; \eta = \left(\frac{\hat{\varepsilon}_1}{\varepsilon_0}\right)^{-1/2} \tag{18}$$

where θ is illustrated in Fig. 1(b). However, our analysis and results presented in Section VII suggest that both coefficients, K_{10} (12) and Γ_{10} (18), lead to very similar results, so we use simpler K_{10} (12) for comparison in the next sections.

It is obvious that an additional image for currents in G_A (17) introduces error of some extent in the low-frequency range. However, the use of images of both current and charge is practically a necessity in EFIE-based solutions, in which it is not possible to define images separately for current and charge, e.g., [5]–[9].

VI. Numerical Results

To examine the accuracy of the approximate expressions of the Green functions given above and to analyze the domain of their applicability, we implemented a set of numerical tests.

We consider an *x*-directed horizontal conductor of radius $a =$ 0.7 cm and lengths $L = 1$, 10, 50, and 100 m, buried at depths $d = 0.3$, 0.5, or 1 m in homogeneous lossy soil, characterized

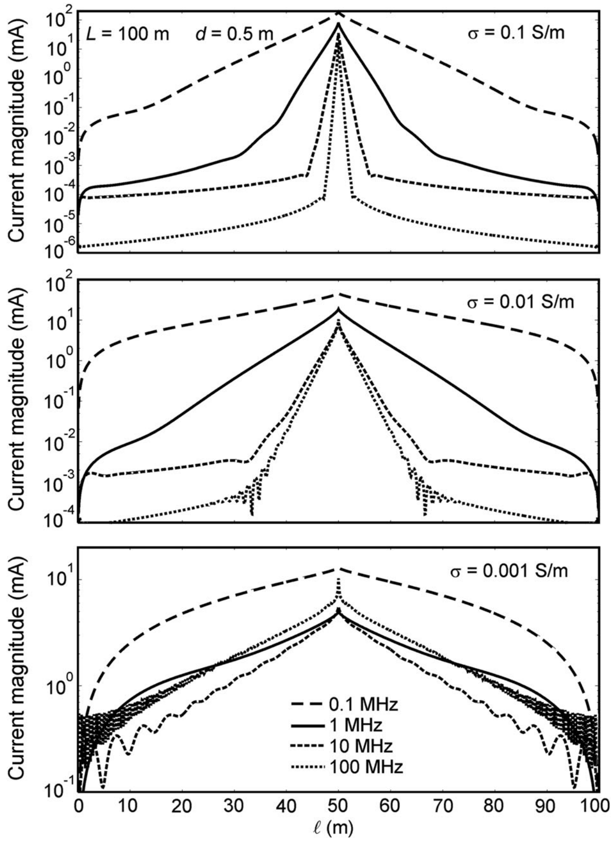

Fig. 2. Current distribution along the 100-m-long wire for antenna type excitation—serial voltage generator 1 V (RMS) at the central point of the wire.

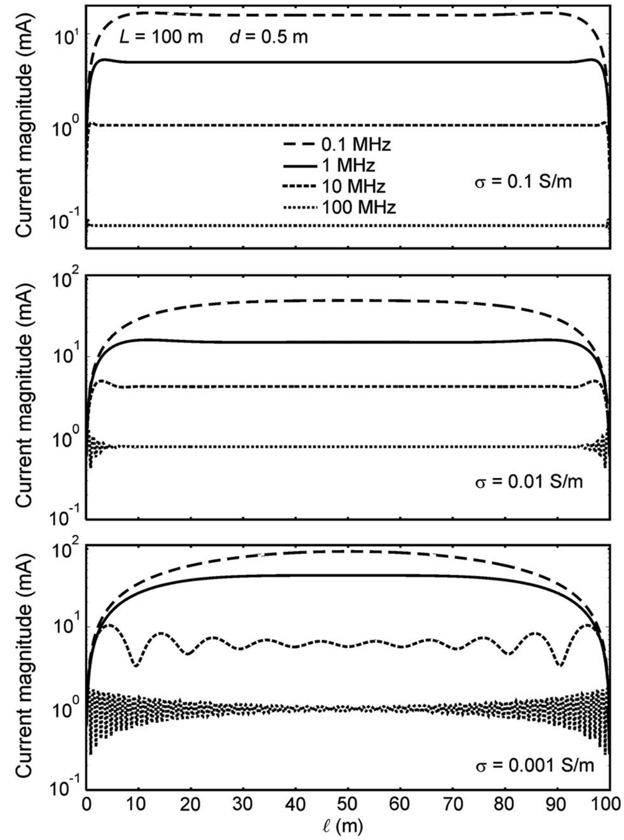

Fig. 3. Current distribution along the 100-m-long wire for scatterer type excitation—illumination by plane wave with 1-V/m electric field tangential to the surface of the wire.

by $\sigma_1 = 0.1$, 0.01, or 0.001 S/m, relative permittivity $\varepsilon_{1r} = 10$, and permeability of vacuum μ_0. The wire is alternatively excited by a harmonic voltage generator with RMS value of 1 V serially connected at the wire central point, or illuminated by a uniform plane wave of normal incidence with 1-V/m electric field tangential to the wire conductor, both in frequency range from dc to 100 MHz. We do not present results for the injection of current via a shunt current generator (which is of interest in grounding analysis), because they are very similar to those presented for voltage generator excitation.

A. Current Distribution

Figs. 2 and 3 illustrate current distribution along a 100-m-long wire for several frequencies (from 0.1 to 100 MHz) and several earth conductivities, for antenna and scatterer type of excitation, respectively. Note that we compared our results in Fig. 2 with FEKO [39] and NEC [40] software using the available options for different excitation models and found that they are in reasonable agreement, especially near the feed point.

We compute the RMS error for the longitudinal current along the conductor [38] as follows:

$$\varepsilon_{\mathrm{rms}} = \left[\frac{\sum\limits_{n=1}^{N} \left| \hat{I}_n^{\mathrm{APP}} - \hat{I}_n^{\mathrm{RIG}} \right|^2}{\sum\limits_{n=1}^{N} \left| \hat{I}_n^{\mathrm{RIG}} \right|^2} \right]^{1/2} \times 100(\%). \qquad (19)$$

Here, $\hat{I}_n^{\mathrm{RIG}}$ is the phasor of the current samples along the conductor computed by a rigorous Sommerfeld integral formulation, and $\hat{I}_n^{\mathrm{APP}}$ is the phasor of the current samples obtained using image approximations. *N* is total number of samples along the conductor.

Figs. 4–7 present the error for the model (17) with images of both current and charge (denoted as "Mod. image"), and for the image model (16) with an image only for the charge (denoted as "Charge img."). Although the current distributions in Figs. 2–3 are quite different for different excitations, the computed frequency characteristics of error for the current in Figs. 4–7 are similar for the different types of excitation (denoted by black and gray lines).

1) Short Conductors (Shorter Than 10 m): Fig. 4 illustrates the $\varepsilon_{\mathrm{rms}}$ error for the current along the 1-m-long horizontal conductor buried at depth $d = 0.5$ m for different soil conductivities.

It is clear that the error for both image models is small (less than 1%) over a wide frequency range. The exception is the case of low-conductivity earth (0.001 S/m), where the upper frequency limit is related to the first resonant frequency. (Please see the discussion in Section VII related to the resonances.)

The effect of the error peaking due to the resonant frequencies is more important for 10-m-long conductors (see Fig. 5) where such frequencies are at much lower frequency ranges. However, the error of both image methods is less than 10% over large frequency ranges [with slightly better results for the method

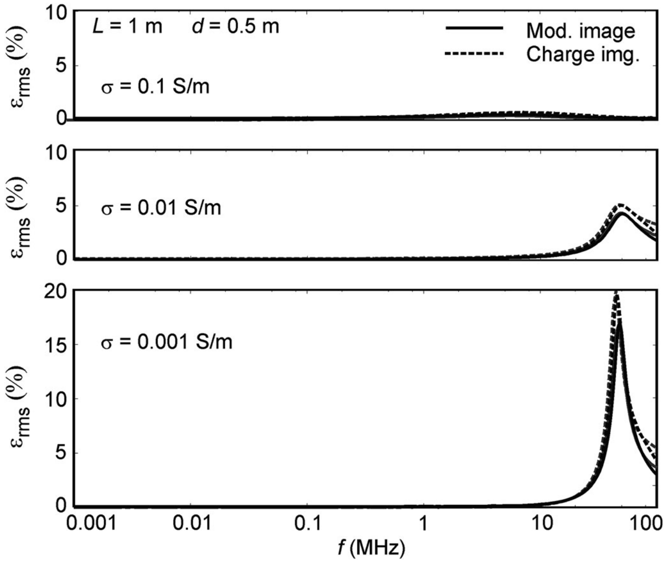

Fig. 4. $\varepsilon_{\rm rms}$ error for current along the 1-m conductor buried at 0.5 m. Black line—voltage generator excitation. Gray line—plane-wave excitation.

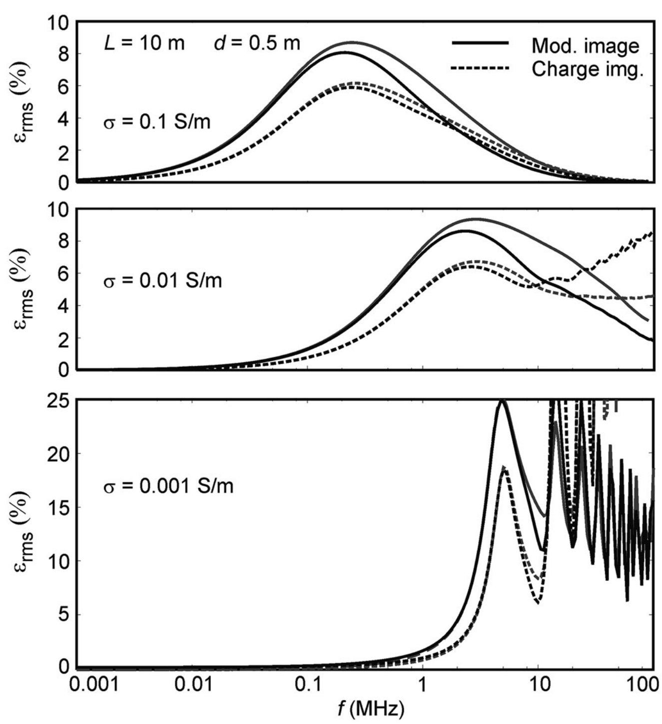

Fig. 5. $\varepsilon_{\rm rms}$ error for current along the 10-m conductor buried at 0.5 m. Black line—voltage generator excitation. Gray line—plane-wave excitation.

with the single image of charge (16)]. The exception is the case of soil with very small conductivity (0.001 S/m) where the behavior is highly resonant and the error is high for frequencies above 1 MHz.

2) Long Conductors (Longer Than 10 m): Figs. 6 and 7 show the error $\varepsilon_{\rm rms}$ for 50- and 100-m-long conductors, respectively. The trend in which the resonant frequency is lower for longer conductors and higher conductivity earth is exhibited by the

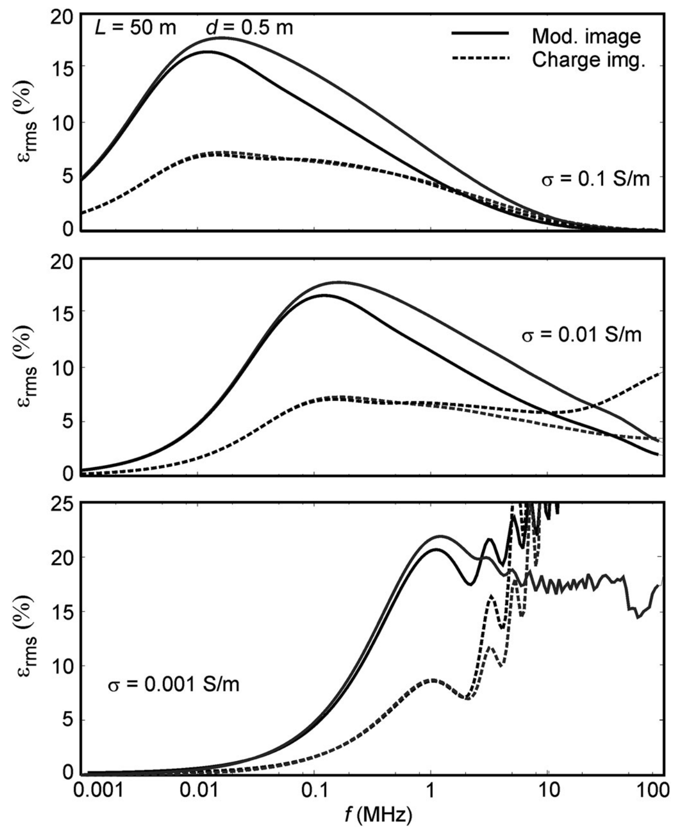

Fig. 6. $\varepsilon_{\rm rms}$ error for current along the 50-m conductor buried at 0.5 m. Black line—voltage generator excitation. Gray line—plane-wave excitation.

large peaks of error in low-frequency ranges. However, in this case, the model with images of both current and charge (17) leads to much larger error than that of the model with the single image of charge (16). The latter model (16) shows a clear advantage: it leads to an error of approximately 5% over the whole considered frequency range (up to 100 MHz) for high-conductivity soil ($\sigma_1 = 0.1$ S/m), up to 10 MHz for medium-conductivity soil ($\sigma_1 = 0.01$ S/m), and up to approximately 1 MHz for low-conductivity soil ($\sigma_1 = 0.001$ S/m).

The error is very large for both models above a few megahertz for very resistive soil ($\sigma_1 = 0.001$ S/m). From the trends in Figs. 6–7, it can be deduced that the upper frequency limit will be lower than 1 MHz for wires longer than 100 m.

B. Input Impedance

We also computed the frequency characteristic of the error for the input impedance seen by the serial voltage generator (computed as the quotient of the generator voltage and current). The error of the input impedance modulus at the voltage generator terminals is

$$\varepsilon_Z = \frac{|Z^{\rm APP}| - |Z^{\rm RIG}|}{|Z^{\rm RIG}|} \times 100(\%). \quad (20)$$

Here, $|Z^{\rm RIG}|$ is the modulus of the impedance computed by the rigorous Sommerfeld integral model, and $|Z^{\rm APP}|$ is the

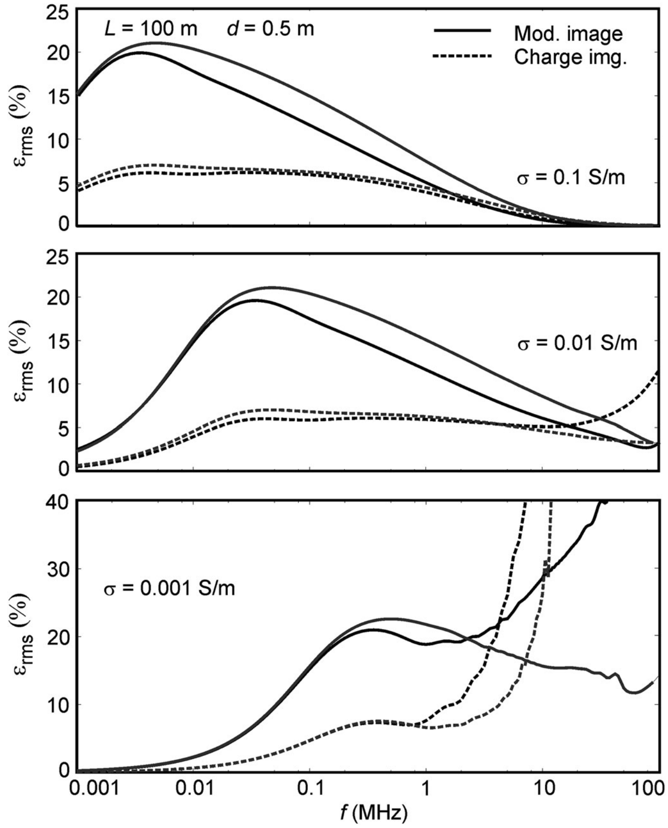

Fig. 7. $\varepsilon_{\rm rms}$ error for the current along the 100-m conductor buried at 0.5 m. Black line—voltage generator excitation. Gray line—plane-wave excitation.

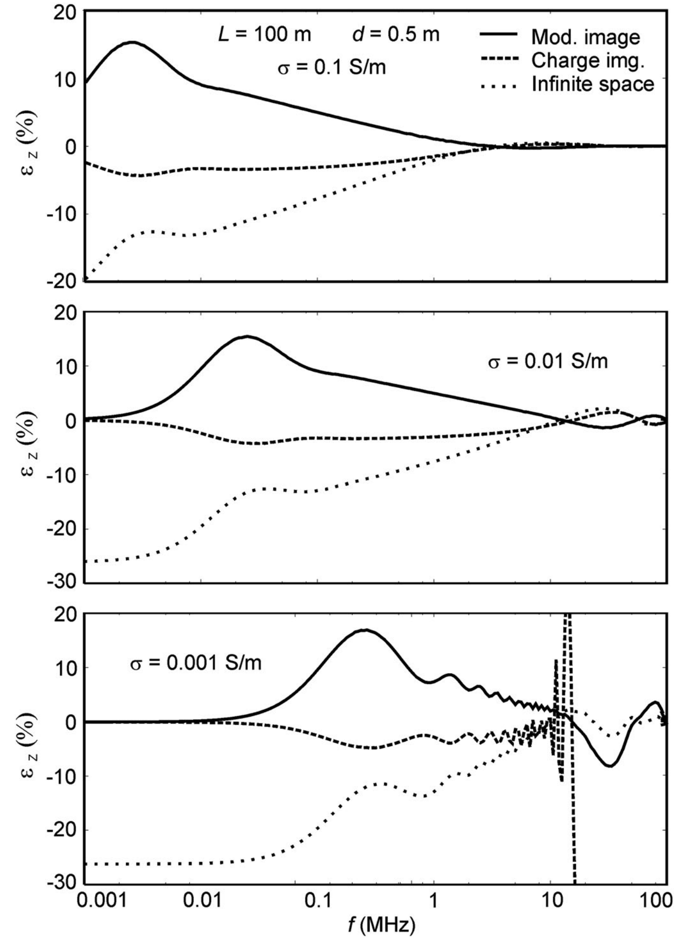

Fig. 8. ε_Z error for impedance of the 100-m conductor at $d = 0.5$ m for different soil conductivities.

modulus of the impedance computed by the approximate image models (16), (17).

We only show the error in impedance for the 100-m wire in Fig. 8 as an example because the frequency characteristics of the error of the impedance for other considered conductor lengths are similar to previously analyzed frequency characteristics of the error of current (as shown in Figs. 4–7).

In addition, here, we show the error when the impedance is computed in infinite space with the characteristics of earth, i.e., when the air/earth interface is completely neglected (dotted line in Fig. 8). In higher conductivity soil (especially for conductivity 0.1 S/m), the air/earth interface clearly loses its influence at high frequencies, and all approximate models lead to an error nearly equal to zero. This is not the case in earth with very small conductivity (0.001 S/m), where the error is high at resonant frequencies.

C. *Influence of the Depth of Burial*

Fig. 9 shows the variation of the $\varepsilon_{\rm rms}$ error with respect to the conductor depth (0.3 and 1 m) for the conductor length of 100 m. (The cases for other conductor lengths are not shown here because the conclusions are similar.)

The results show that depth of burial has a significant influence on the error of the image model with both images for current and charge (17). The error is higher for the shallow conductor burial depth ($d = 0.3$ m) than for the deeper burial depth ($d = 1$ m). The sensitivity of the error to the burial depth is considerably smaller for the model with the image only for the charge (16).

VII. Validation of the Computations

Validation of the presented rigorous Sommerfeld integral solution may be found elsewhere, e.g., [14], [33]. We validated our computations of $\varepsilon_{\rm rms}$ error (19) for the current by comparison with NEC software [40]. In NEC, we computed error of the reflection coefficient approximate method related to its Sommerfeld rigorous solution. As shown in Figs. 10 and 11, the results for $\varepsilon_{\rm rms}$ error of here analyzed image model (17) are in reasonable agreement with $\varepsilon_{\rm rms}$ error results calculated by NEC. Note that the here analyzed image model (17) uses quasi-static Fresnel reflection coefficient for a normal plane-wave K_{10} (12), while NEC uses reflection coefficient for oblique plane-wave Γ_{10} (18). Nevertheless, both approaches lead to similar results, and, therefore, to similar errors in computation of the current distribution.

We also compared the ε_Z error (20) computed with our rigorous Sommerfeld integral model and with FEKO software [39], revealing agreement to within less than one percent.

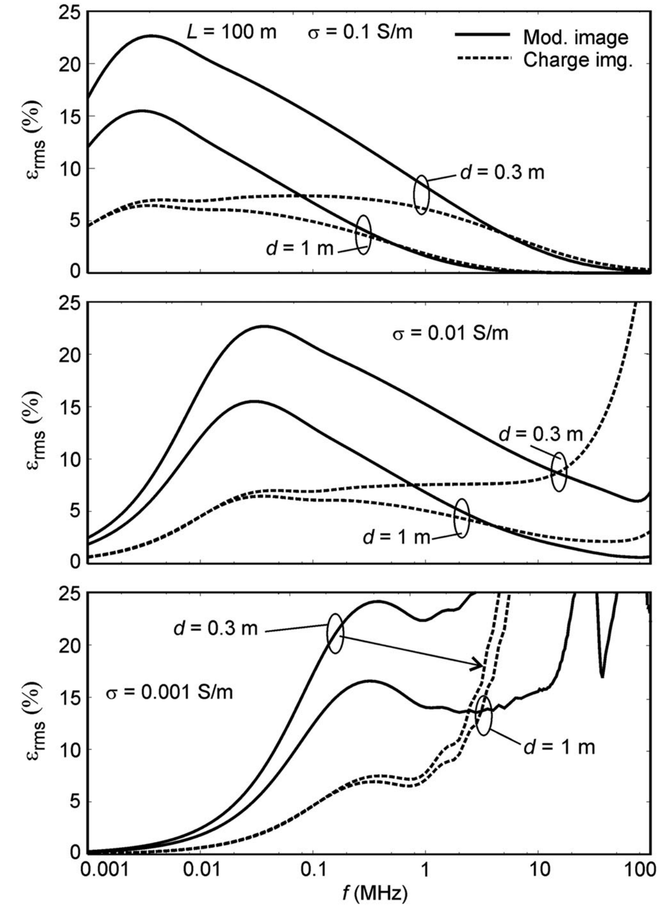

Fig. 9. Error for current along the 100-m conductor at depths of burial $d = 0.3$ m and $d = 1$ m for different soil conductivities.

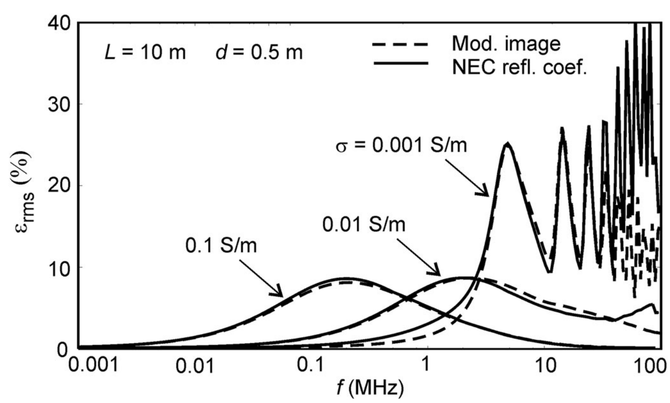

Fig. 10. Comparison of the error for current with NEC for the 10-m-long wire.

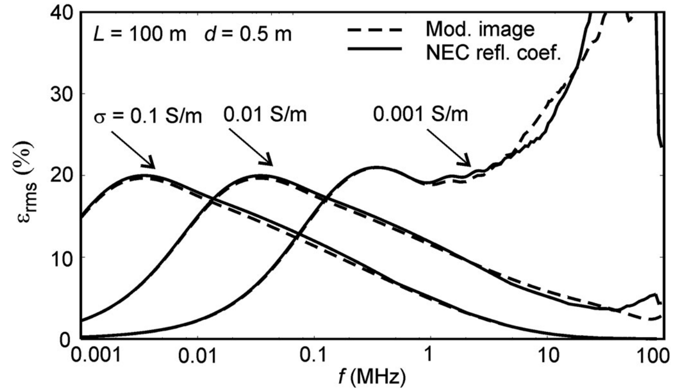

Fig. 11. Comparison of the error for current with NEC for the 100-m-long wire.

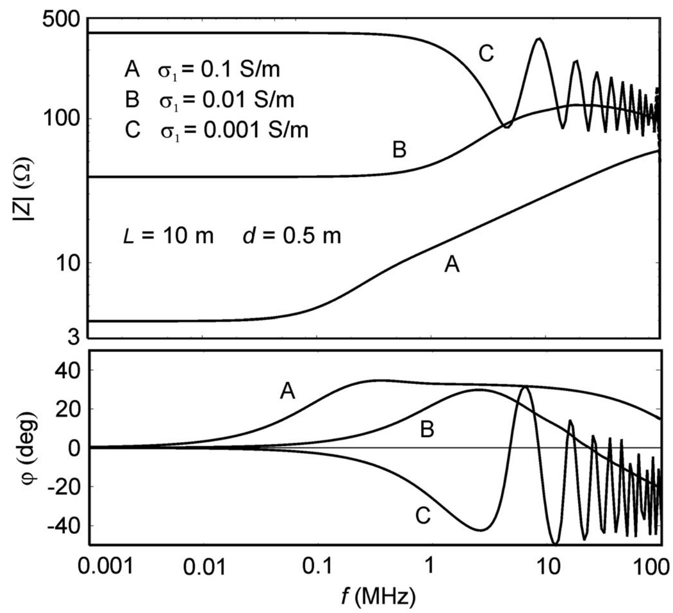

Fig. 12. Modulus and phase of the harmonic impedance at the terminals of the serial voltage generator at the wire's middle point.

VIII. Discussion

The frequency characteristics of the error of the image model analyzed in previous sections are related to resonant behavior. For example, Fig. 12 shows the frequency characteristic of the impedance of the 10-m-long wire. This characteristic has a clear resonant behavior for $\sigma_1 = 0.001$ S/m, while for more conductive earth ($\sigma_1 = 0.1$ S/m and $\sigma_1 = 0.01$ S/m), the resonances are suppressed. In the latter case, there exists a transition frequency at which impedance changes its behavior from dominantly resistive to dominantly inductive (change in magnitude from nearly constant to rising in Fig. 12).

The maximum of the error occurs at frequencies that are somewhat larger than the transition frequency, and in the case of $\sigma_1 = 0.001$ S/m, the transition occurs at frequency somewhat larger than the frequency of the first minimum of the impedance modulus. These frequencies also correspond approximately with the first maxima of the impedance phase.

Such frequencies (at which the maximum of the error occurs) can be approximately determined by solving for f in

$$\lambda_1 \approx 3\ell/2 \tag{21}$$

where λ_1 is the wavelength in soil [41]:

$$\lambda_1 = \frac{1}{f\sqrt{\mu_0\varepsilon_1}}\left\{\frac{1}{2}\left[\sqrt{1+\left(\frac{\sigma_1}{2\pi f\varepsilon_1}\right)^2}+1\right]\right\}^{-1/2} \tag{22}$$

The computation results show that differences between the computed current by the image methods and the rigorous Sommerfeld integral method are the largest at and near the above-mentioned resonance-related frequencies and are smaller away from these frequencies.

It appears that an additional image for current in the method with both images for current and charge (17) leads to a large error at the frequencies described above (that are in the low-frequency range for long conductors and in higher conductivity earth). However, there exist cases at high frequencies, especially for soil of high resistivity [$\sigma = 1000$ S/m, Fig. 7(c)], where this method behaves better than the method with the image only for the charge. This result might be related to the fact that components of the field due to current and charge are opposite to each other, with errors of both images that mutually cancel each other. One exception is the case of high-conductivity soil (0.1 S/m), where the field at high frequencies is localized near the conductor (skin depth of approximately 0.2 m at 100 MHz) and the air/earth interface has no influence.

IX. Conclusion

The following conclusions are reached for the application of the image (or reflection coefficient) method for computation of the current in buried horizontal wires of finite length.

1) For conductors shorter than 10 m, both image models lead to errors of less than 10% over wide frequency ranges (up to 100 MHz in the here-considered frequency range). An exception is the case of earth with very low conductivity (0.001 S/m or smaller), where the upper frequency limits is related to the first resonant frequency (approximately 20 MHz).
2) For conductors longer that 10 m, a distinction should be made between solutions that implement the image model. Solutions that use the model with images of both current and charge (often referred in literature as "modified image" method, e.g., [8], or "reflection coefficient" method, e.g., [9]), such as EFIE-based solutions (e.g., Pocklington integral equation), lead to high error (greater than 20%) in the low-frequency range. Solutions that use model with the image only for the charge, such as MPIE based solutions, e.g., [14], lead to error of approximately 5% up to some upper limit frequency.
3) Such upper frequency limit is up to 100 MHz (in the here-considered frequency range) for very high-conductivity earth (0.1 S/m), up to approximately 10 MHz for medium-conductivity soil ($\sigma_1 = 0.01$ S/m), and up to approximately 1 MHz for low-conductivity soil ($\sigma_1 = 0.001$ S/m).
4) A smaller depth of burial increases the error of the model with both images for current and charge, while a much smaller effect is found for the model with the image only for the charge.
5) The errors of the image models are similar for different forms of the reflection coefficient (for normal and oblique incidence) and for different types of excitation (with serial voltage generator, injected current by shunt current generator and illumination by plane wave).

Acknowledgment

The authors would like to thank the three anonymous reviewers, whose comments and suggestions allowed us to improve this paper.

References

[1] R. W. P. King and G.S. Smith, *Antennas in Matter*. Cambridge, MA, USA: MIT Press, 1981.
[2] J. R. Wait, *Geo-Electromagnetism*. New York, NY, USA: Academic, 1982.
[3] F. M. Tesche, M. Ianoz, and T. Karlsson, *EMC Analysis Methods and Computational Models*. New York, NY, USA: Wiley, 1997.
[4] E. D. Sunde, *Earth Conduction Effects in Transmission Systems*, 2nd ed. New York, NY, USA: Dover, 1968
[5] R. W. P. King, "Antennas in material media near boundaries with application to communication and geophysical exploration, Part I: The bare metal dipole," *IEEE Trans. Antennas Propag.*, vol. AP-34, no. 1, pp. 483–489, Apr. 1986.
[6] F. P. Dawalibi and R. D. Southey, "Analysis of electrical interference from power lines to gas pipelines," *IEEE Trans. Power Del.*, vol. 5, no. 1, pp. 415–421, Jan. 1990.
[7] F. Han, S. Sali, and W. T. Smith, "Response of underground multiconductor cable systems to external fields illumination," *IEE Proc. Sci. Meas. Technol.*, vol. 143, no. 2, pp. 137–142, Mar. 1996.
[8] L. Grcev, "Computer analysis of transient voltages in large grounding systems," *IEEE Trans. Power Del.*, vol. 11, no. 2, pp. 815–823, Apr. 1996.
[9] D. Poljak, V. Doric, F. Rachidi, K. Drissi, K. Kerroum, S. V. Tkachenko, and S. Sesnic, "Generalized form of telegrapher's equations for the electromagnetic field coupling to buried wires of finite length," vol. 51, no. 2, pp. 331–337, May 2009.
[10] J. R. Wait, *Electromagnetic Wave Theory*. New York, NY, USA: Harper & Row, 1985.
[11] L. Grcev, "Computation of transient voltages near complex grounding systems caused by lightning currents," in *Proc. IEEE Int. Symp. Electromagn. Compat.*, 1992, pp. 393–400.
[12] V. Arnautovski-Toseva and L. Grcev, "Image and exact models of a vertical wire penetrating a two-layered earth," *IEEE Trans. Electromagn. Compat.*, vol. 53, no. 4, pp. 968–976, Nov. 2011.
[13] A. Banos and J. P. Wesley, *The Horizontal Electric Dipole in a Conducting Half-Space*. Berkeley, CA, USA: Scripps Inst. Oceanography, Marine Physics Lab., Univ. California, Sep. 1953, ch. 4, Rep. 53–33.
[14] V. Arnautovski-Toseva and L. Grcev, "Electromagnetic analysis of horizontal wire in two-layered soil," *J. Comput. Appl. Math.*, vol. 168, nos. 1/2, pp. 21–29, Jul. 2004.
[15] L. Grcev and V. Arnautovski, "Comparison between simulation and measurement of frequency dependent and transient characteristics of power transmission line grounding," in *Proc. Int. Conf. Lightning Protection*, Birmingham, U.K., 1998, pp. 524–529.
[16] L. Grcev, "Lightning surge efficiency of grounding grids," *IEEE Trans. Power Del.*, vol. 26, no. 3, pp. 1692–1699, Jul. 2011.
[17] L. Grcev, B. Markovski, V. Arnautovski-Toseva, and K. E. K. Drissi, "Transient analysis of grounding systems without computer," in *Proc. Int. Conf. Lightning Protection*, Vienna, Austria, 2012, pp. 1–6.
[18] J. R. Wait, "The false image of a line current within a conducting halfspace," *IEEE Trans. Electromagn. Compat.*, vol. 39, no. 3, pp. 266–267, Aug. 1997.
[19] J. R. Wait, "Comment: Response of underground multiconductor cable systems to external fields illumination," *IEE Proc. Sci. Meas. Technol.*, vol. 144, no. 6, pp. 294–295 , Nov. 1997.
[20] F. Han, "Validity of ETLEs model for coupling to underground transmission systems, reply to comment on response of underground multiconductor cable systems to external fields illumination," *IEE Proc. Sci. Meas. Technol.*, vol. 144, no. 6, pp. 294–295, Nov. 1997.
[21] J. R. Wait, "Comment: Response of underground multiconductor cable systems to external fields illumination," *IEE Proc. Sci. Meas. Technol.*, vol. 146, no. 1, pp. 54–55, Jan. 1999.
[22] S. Sali, "Reply to comment on Response of underground multiconductor cable systems to external fields illumination," *IEE Proc. Sci. Meas. Technol.*, vol. 146, no. 1, pp. 54–55, Jan. 1999.
[23] A. Sommerfeld, *Partial Differential Equations in Physics*. New York, NY, USA: Academic, 1949.
[24] A. Banos, *Dipole Radiation in the Presence of a Conducting Half-Space*. Oxford, U.K.: Pergamon, 1966.

[25] G. Burke and E. K. Miller, "Modeling antennas near to and penetrating a lossy interface," *IEEE Trans. Antennas Propag.*, vol. AP-32, no. 10, pp. 1040–1049, Oct. 1984.
[26] I. V. Lindell, *Methods for Electromagnetic Field Analysis*. New York, NY, USA: Wiley-IEEE, 1992.
[27] A. Shoory, R. Moini, and S. H. H. Sadeghi, "Direct use of discrete complex image method for evaluating electric field expressions in a lossy half space," *IET Microw. Antennas Propag.*, vol. 4, no. 2, pp. 258–268, 2010.
[28] D. Cavka, N. Mora, and F. Rachidi, "A comparison of frequency-dependent soil models: Application to the analysis of grounding systems," *IEEE Trans. Electromagn. Compat.*, vol. 56, no. 1, pp. 177–187, Feb. 2014.
[29] R. F. Harrington, *Field Computation by Moment Method*. New York, NY, USA: Wiley-IEEE, 1993.
[30] D. C. Kuo, H. H. Chao, J. R. Mautz, B. J. Strait, and R. F. Harrington, "Analysis of radiation and scattering by arbitrary configurations of thin wires," *IEEE Trans. Antennas Propag.*, vol. 20, no. 6, pp. 814–815, Nov. 1972.
[31] L. Grcev and Z. Haznadar, "A novel technique of numerical modelling of impulse current distribution in grounding systems," in *Proc. Int. Conf. on Lightning Protection*, Graz, Austria, 1988, pp. 165–169.
[32] L. Grcev and F. Dawalibi, "An electromagnetic model for transients in grounding systems," *IEEE Trans. Power Del.*, vol. 5, no. 4, pp. 1773–1781, Oct. 1990.
[33] J. R. Mosig and F. E. Gardiol, "A dynamic radiation model for microstrip structures," in *Advances in Electronics and Electron Physics*, vol. 59, P. W. Hawkes, Ed. New York, NY, USA: Academic, 1982, pp. 139–237.
[34] J. R. Mosig, "Integral equation technique," in *Numerical Techniques for Microwave and Milimeter-Wave Passive Structures*, T. Itoh, Ed. New York, NY, USA: Wiley, 1989, pp. 133–213.
[35] K. A. Michalski, "The mixed-potential electric field integral equation for objects in layered media," *Arch. Elek. Ubertragung.*, vol. 39, no. 5, pp. 317–322, Sep./Oct. 1985.
[36] K. A. Michalski and J. R. Mosig, "Multilayered media Green functions in integral equation formulations," *IEEE Trans. Antennas Propag.*, vol. 45, no. 3, pp. 508–519, Mar. 1997.
[37] W. C. Chew, *Waves and Fields in Inhomogeneous Media*. New York, NY, USA: Wiley-IEEE, 1995.
[38] R. Poggio Bevensee and E. K. Miller, "Evaluation of some thin wire computer programs" in *Proc. IEEE Antennas Propag. Symp.*, Jun. 1974, vol. 12, pp. 181–184.
[39] EM Software and Systems-S.A. (Pty) Ltd., FEKO, Stellenbosch, South Africa. [Online]. Available: http://www.feko.info
[40] G. J. Burke, "Numerical electromagnetics code NEC-4 method of moments," Lawrence Livermore Nat. Lab., Livermore, CA, USA, Tech. Rep. UCRL-MA-109338, 1992.
[41] C. A. Balanis, *Advanced Engineering Electromagnetics*. New York, NY, USA: Wiley, 1989.

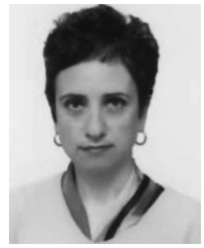

Vesna Arnautovski-Toseva (M'89) was born in Zagreb, Croatia, in 1961. She received the Dipl.Ing., M.S., and Ph.D. degrees in electrical engineering from the Saints Cyril and Methodius University, Skopje, Macedonia, in 1986, 1992 and 2004, respectively.

In 2010–2012, she was with Institute Pascal, Blaise Pascal University, Clermont-Ferrand, France. Since 1989, she has been a Member at the Faculty of Electrical Engineering and Information Technologies, Saints Cyril and Methodius University, where she is also an Associate Professor. Her research interests include EMC, computational electromagnetic applied to high frequency and transient grounding, lightning, and EMC in power line communications.

Dr. Arnautovski-Toseva is a Member of the Macedonian CIGRE Study Committee C3.

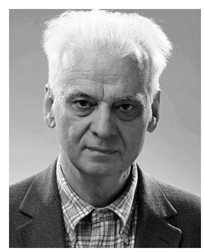

Leonid Grcev (M'84–SM'97–F'13) received the Dipl.Ing. degree in electrical engineering from the Saints Cyril and Methodius University, Skopje, Macedonia, in 1978, and the M.S. and Ph.D. degrees in electrical engineering from the University of Zagreb, Zagreb, Croatia, in 1982 and 1986, respectively.

In 1978, he was with the Telecommunications Department, Electric Power Company, Skopje. He is currently a Professor with the Faculty of Electrical Engineering and Information Technologies, Saints Cyril and Methodius University, where he has been since 1988. He has been a Visiting Professor at the Technical University of Aachen, Aachen, Germany, the Eindhoven University of Technology, Eindhoven, The Netherlands, and the Swiss Federal Institute of Technology, Lausanne, Switzerland. He was responsible for several international projects related to electromagnetic compatibility (EMC). He is an Author and Coauthor of many scientific papers published in peer-reviewed journals and presented at international conferences. He is the principal Author of TRAGSYS software for grounding analysis. His research interests include EMC, high frequency and transient grounding, and lightning.

Dr. Grcev is an IEEE PES Distinguished Lecturer. He was elected to full membership of the Macedonian Academy of Sciences and Arts in 2009.